

Full Length Research Paper

Geochronological dating and stratigraphic sequences of Harrat Lunayyir, NW Saudi Arabia

Al-Amri A. M.^{1*}, Fnais M. S.¹, Kamal Abdel-Rahman¹, Mogren S.² and Al-Dabbagh M.¹

¹Department of Geology and Geophysics, King Saud University, Riyadh, Saudi Arabia.

²Department of Geology and Geophysics & Empty Quarter Research Chair, King Saud University, Riyadh, Saudi Arabia.

Accepted 4 May, 2012

Harrat Lunayyir is a basaltic volcanic field in NW Saudi Arabia. Lava flows are basaltic to basanitic in composition, and the Holocene flows are alkali olivine basalts. The volcanic field contains about 50 cones that were constructed on Precambrian crystalline rocks along an N-S axis. The dominantly basaltic lavas of Harrat Lunayyir have been divided based on their erosion characteristics into two major units – an older Tertiary unit (Jarad basalt) and a younger Quaternary unit (Maqrah basalt). The Quaternary Maqrah basalt has been subdivided into five stratigraphic subunits, Qm1 and Qm2 forming the Lower Maqrah basalt and Qm3, Qm4, and Qm5 forms the Upper Maqrah basalt. In 2009, a 3-km-long rupture in Harrat Lunayyir and lengthened to 8 km. Satellite radar images suggested that the most likely cause of this fault was magma intruding vertically along a 10-km-long fracture. The regional stress field deduced from the orientation of the observed dike indicates NE - SW tension, which is also indicated by focal mechanism solutions with normal faulting with two major structural trends of NE-SW and NW-SE. These trends are consistent with the orientation of the opening of the Red Sea and with regional tectonics of Arabian-African rifting. Moreover, these results show that the Red Sea ridge stress field extends at least 200 km from the rift axis into the Arabian plate. Prior to this study, estimates of the ages of the samples ranged from Tertiary to Quaternary. This work places the ages of all samples firmly in the Quaternary period. ⁴⁰Ar/³⁹Ar age determinations have been produced for six samples. Most of these are fine-grained enough that whole-rock fragments were chosen for irradiation. The precision of the ages calculated in this study are limited by the small amounts of radiogenic argon compared to the larger amounts of non-radiogenic, or background argon typical in basaltic whole rocks of this age. The discrepancies in ages and stratigraphic position are due to the small amounts in accumulated argon over the relatively very short period of time. In general, this study shows that volcanic activity at Harrat Lunayyir started about 500,000 years ago. There must have been a substantial time between the lowest unit (which has previously been assigned a tertiary age) and youngest so that an unconformity has been developed. The latest activity could have taken place at about 5000 years ago.

Key words: Geochronological dating, Harrat Lunayyir, age determinations, Maqrah basalt, Saudi Arabia.

INTRODUCTION

Lunayyir is undergoing a volcano-seismic crisis long time ago where a remarkable amount of microseismic activity and prolific volcanism have been reported (Kinkar et al., 1994b; Roobol et al., 1994; Roobol and Al-Rehaili, 1997).

This volcano-seismic crisis repeated, recently, with a commencement of swarms at shallow depths along with the presence of fumaroles indicates a possible new cycle of activity (Al-Amri and Fnais, 2009). Such events can last for a year or two and then die out. Alternatively they can continue and escalate leading to felt earthquakes (probably no greater than magnitude 5) and result in a basaltic eruption similar to that which occurred near Al

*Corresponding author. E-mail: seismology333@gmail.com.

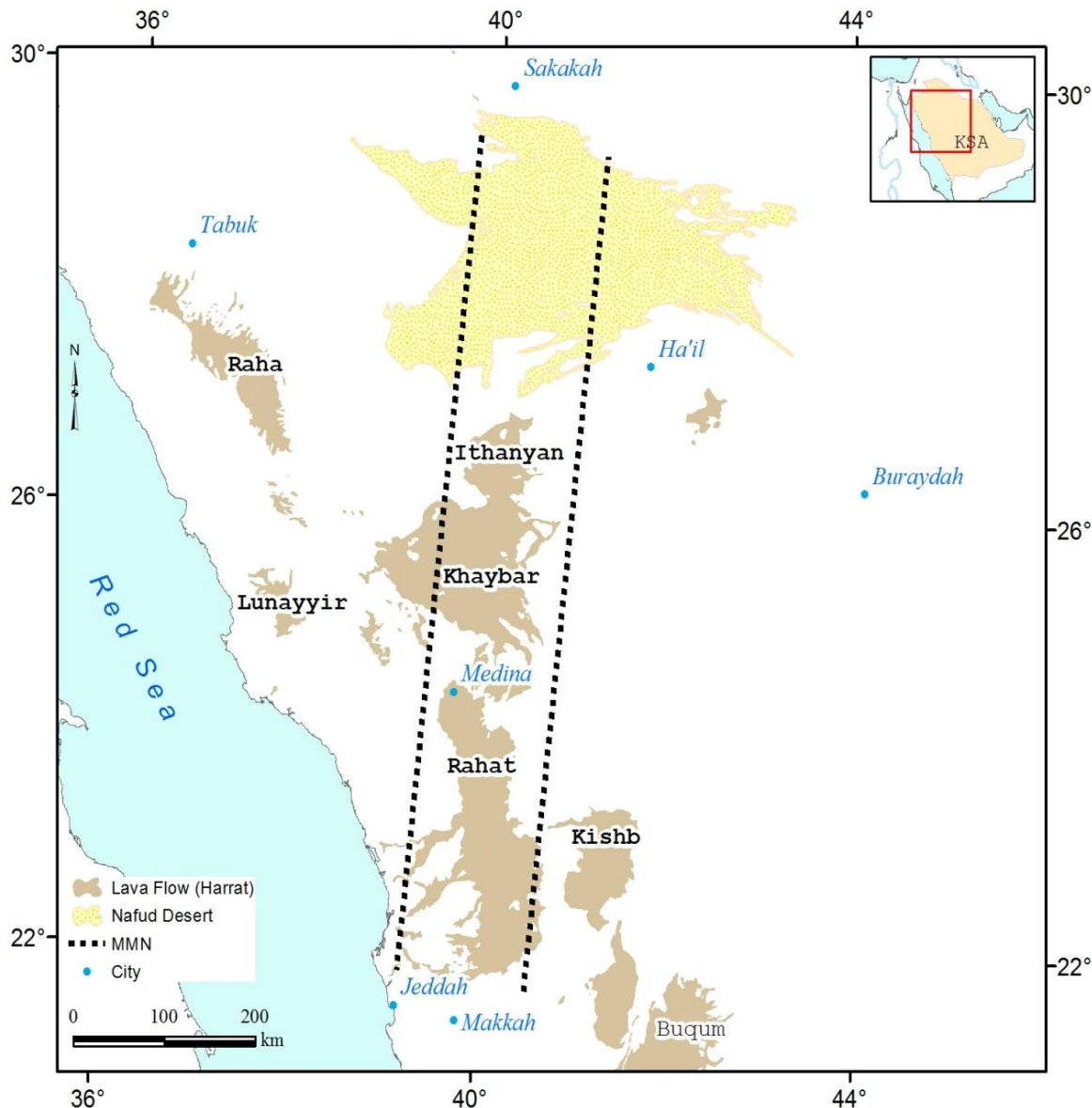


Figure 1. Location map of Harrat Lunayyir and MMN line.

Madinah city in 1256 A.D. / 654 A.H. At the Hawaiian Volcanic Observatory the passage of basaltic magma has been followed as it rises from depths of around 50 km using seismometers, until eruption around ten months later (Trilling et al., 2010). These basaltic eruptions are considered the safest type of volcanic activity and do not usually involve the loss of life and the lava flows can today be diverted away from settlements by building earth banks.

During the late Oligocene and early Miocene, the Arabian Shield was disrupted by the development of the Red Sea and Gulf of Aden rifts, and from the mid-Miocene to the present, the region experienced volcanism and uplift. The approximate 600 km long

Makkah-Madinah-Nafud (MMN) volcanic line (Figure 1), consisting of Harrats Rahat, Khaybar, and Ithnayn, is the proposed surface expression of the plume-related intraplate volcanism (Moufti and Hashad, 2005) and northward propagating nascent rift system (Camp et al., 1989, Camp and Roobol, 1992). The existence of a mantle plume beneath the western part of the Arabian plate beneath the Al-Madinah Al-Munawwarah region including Harrat Lunayyir has been suggested (Moufti and Hashad, 2005; Al-Damegh et al., 2005; Julia et al., 2003; Benoit et al., 2003; Daradich et al., 2003). The last two historic volcanic eruptions, close to the city of Al-Madinah Al-Munawwarah occurred at about 641 A.D. and then again at 1256 A.D.

Harrat Lunayyir is located NW of Al-Madinah Al Munawwarah, north of Yanbu and in the immediate vicinity of the town of Al Ays between latitudes 25°.1 to 25°.17 N and longitudes 37°.45 to 37°.75 E, occupying a surface area of about 3575 Km² (Figure 1). The volcanic field is oriented northwest–southeast and, morphologically, there are great variations in the altitudes between hills and wadies through the area. The region is characterized by geothermally groundwater, with temperatures up to 32°C measured in April 2007 before the earthquake swarm began. Farmers in the Harrat Lunayyir area have reported seeing steam in many places on cold winter mornings. The geothermal anomalies and reports of stream were first noted by Saudi Geological Survey staff in 2001.

Historical records of seismic (Poirier and Taher, 1980; Barazangi, 1981) and volcanic activity suggest that within-plate volcanism has resulted in at least 21 eruptions in the Arabian Peninsula during the past 1500 years (Camp et al., 1987) including one at Harrat Lunayyir about 1000 years ago. The eruption in 1256 near the holy city of Madinah, Saudi Arabia is of particular historical and contemporary importance, for the lava flowed to within 8 km of the ancient city (Camp et al., 1987). Since 1985, instruments have recorded frequent seismic activity within and around the City of Al-Madinah Al-Mounwwarah, especially the recent 1999 earthquake swarms (SGS, 2005) and the ground deformation (Kinkar et al., 1994b). The signs of geothermal anomalies such as fumarolic emission and elevated well-water temperature within the city limits and also on Harrat Lunayyir indicate the dynamic role of melt production beneath the Harrat Al-Madinah (Roobol et al., 1994) and Harrat Lunayyir.

The origin of the seismic waves from volcanic activities can be attributed to two fundamentally different sources (Zobin, 2003; Zobin et al., 2011). These are the pressure variations associated with the unsteady fluid flow of magma and volatiles generating volcanic tremors, and the stress changes by sudden dislocations of shear/tensile cracks within the rigid parts of the volcanoes causing volcanic earthquakes. Frequently, volcanic eruptions are reported to have been preceded by strong earthquakes or earthquake swarms occurring in a focal zone below the subsequent eruption. Pallister et al. (2010) document a surface fault rupture of 8 km length with 91 cm of offset in Harrat Lunayyir and modeled the surface deformation by the shallow intrusion of a northwest-trending, sub-surface dike that is about 10 km long. Seismic waves generated during the earthquakes exhibit overlapping very low- and high-frequency components. Pallister et al. (2010) interpret the low frequencies to represent intrusion of magma and the high frequencies to represent fracturing of the crystalline basement rocks. Rather than extension being accommodated entirely by the central Red Sea rift axis, these authors suggest that the broad deformation observed in

Harrat Lunayyir indicates that rift margins can remain as active sites of extension throughout rifting.

Jonsson et al. (2010) conclude that the deformation is caused by a near-vertical dike intrusion with a NW-SE orientation, parallel to the Red Sea rift, and the intruded volume is of the order of 0.1 km³. The dike triggered faulting on graben-forming normal faults. The shallowest part of the dike appears to have reached within only 2 to 3 km of the surface, right below the narrowest part of the graben and under an area with a number of cinder cones from previous volcanic events. Geological observations show a roughly 3-km-long rupture has opened up in the area and lengthened to 8 km during the swarm activity (Figure 2). Satellite radar images suggest the most likely cause of this fault to be magma intruding upward over a 10-km-long stretch. Baer and Hamiel (2010) derived the vertical and rift-perpendicular deformation, which adds up to a maximum surface extension of 1.5 m across the rift and subsidence of 0.8 m. The far-field deformation is dominated by the dike opening, whereas the near-field displacements are mostly associated with movements along the faults. The deformation during the rifting event was controlled by a 12-km-long dike, with maximum thickness of 2.5 m, and two normal faults that bound a wedge-shaped graben above the dike.

In order to fully understand the seismicity and volcanic characteristics of Harrat Lunayyir and its relation to regional tectonics, the main objective of this paper is to produce a geological map of the Harrat Lunayyir lava field, identify volcanic stratigraphy, age of past eruptions, mineralogical and chemical characteristics of the lavas. Satellite images of the lava fields in western Saudi Arabia, particularly in the northern part of Harrat Lunayyir, can be used to verify and monitor volcanic activity and relate to geologic and geographic information in this area. The sites of youngest volcanic activity are most likely for near future activity.

GEOLOGIC SETTING

The western part of the Arabian shield is made up of three major accreted tectonostratigraphic terranes (Asir, Jeddah and Hijaz) consisting mainly of various metamorphosed layered volcano-sedimentary assemblages of older Baish, Bahah and Jeddah groups (950 to 800 Ma) and younger Halaban (Hulayfah) and Al Ays groups (800 to 650 Ma) with arc-related plutonic rocks of diorite to tonalite compositions, which generally have intrusive relationship with the volcano-sedimentary sequences (Stoeser and Camp, 1985; Johnson, 2000). The great lava fields or harrats of flood basalt erupted on the western shield during the Late Oligocene and Early Miocene and at the same time, a 2000 km long continental rift valley developed along the future Red Sea axis. During the late Early Miocene time, the Red Sea opened initially at a rate of 4.4 cm/yr while swarms of



Figure 2. Surface fault ruptures formed in Harrat Lunayyir during the 2009 earthquake swarm. The ground displacements in the soft sediments of the foreground are greater than in basement rocks of the background.

tholeiitic dikes, gabbro, and granophyres plutonic rocks were intruded into the rift sedimentary and volcanic rocks at the newly formed continental margin.

Geologically, Harrat Lunayyir is a very young volcanic region composed of late Neogene and Quaternary basaltic lavas and pyroclastics directly overlying deeply eroded Neoproterozoic rocks of the Arabian Shield (Johnson, 2000). The basement rocks surrounding Harrat Lunayyir belong to two different lithostratigraphic units: Midyan terrane located NW and Hijaz terrane in SE (Johnson, 1998). A complex of fault-bounded belt of ultramafic to mafic ophiolitic rocks known as Jabal Wask ophiolite lies between these two terranes and forms the Yanbu suture.

The oldest lavas of Harrat Lunayyir are most probably Pliocene in age, while the younger Quaternary lavas are much fresher, black in color and show a rugged surface topography that is unaffected by erosion. These younger lavas were erupted during at least five stages of volcanic activity. The first two stages produced very fluid basic lavas, which were able to travel long distances (more than 30 km), while the last three stages erupted more

viscous and more felsic lavas that are lighter in color, and which cover a more restricted area. The fourth episode was associated with additional explosive activity which gave birth to numerous cinder cones formed from pyroclastics deposits.

The Cenozoic to recent basaltic lava fields (harrats) of Saudi Arabia are resting directly on the so-called stable Precambrian Arabian Shield. Harrat Lunayyir is characterized by Cenozoic flood basaltic flows which can be differentiated into different cycles of metamorphism and tectonism with variable intensities during Tertiary-Quaternary age. It suffered from series of volcanic eruptions that took place along related fissures and cinder cones forming a zone of N-S and NW-SE trends. Magmatic lavas reached the ground surface through the prevailing deep cracks and fissures. These basaltic flows have been exposed throughout western Saudi Arabia since Miocene time and extend to about 150 to 200 km inland from the Red Sea coast.

Tectonically, Harrat Lunayyir was affected by two episodes of tectonic movements synchronized with the Red Sea floor spreading through pre-early Miocene rifting

period (Girdler, 1969). Furthermore, it is controlled to great extent by the regional stress regime of the western Arabian plate associated with the Cenozoic development of the Red Sea. Harrat Lunayyir probably faulted during Cenozoic rift time where the up arching period was parallel to the Red Sea coast. During Late Miocene – Pliocene, the alkalic basalt invaded into the Harrat Lunayyir. According to the above-mentioned, there are different fault trends prevailing the area and oriented NE-SW, NNW-SSE, and NW-SE (Figure 3).

Detailed maps of the geological formations determined from field investigation (Figure 4) indicated that the Precambrian rocks occupy the northern and the southern parts together with the eastern periphery of the mapped area. In the central zone the Precambrian rocks form isolated inliers. During volcanic activity episodes the relief of the Precambrian rock was high enough to hinder the basalt flow westwards. Field observations lead to the identification of the following volcanic units (young to old):

- Historic to late prehistoric lava flows.
- Prehistoric lava flows and scoria cones.
- Non eroded lava flows and scoria cones.
- Eroded lava flows and scoria cones.
- Eroded lava flows.
- Unconformity.
- Tertiary basalt.

LUNAYYIR STRATIGRAPHY

The dominantly basaltic lavas of Harrat Lunayyir have been divided on the basis of their erosional characteristics into two major formations: older (Tertiary) Jarad basalt, and younger (Quaternary) Maqrah basalt. The Jarad basalt (stratigraphic code Tj) is named after a large area of eroded Tertiary basalt with a prominent eroded red scoria cone of Jabal Abu Jarad, which rises to 1169 m (1:50,000 topographic sheet Hiran No. 3724-11). The Maqrah basalt (stratigraphic code Qm) is named after a large area of Quaternary basalt (which may be the historic eruption of around 1000 AD and is named Harrat Maqrah on 1:50,000 topographic sheet Abar Al Hurayyidah – No. 3725-22). The Quaternary Maqrah basalt has been subdivided into five stratigraphic subunits; Qm1 and Qm2 forming the Lower Maqrah basalt while Qm3, Qm4, and Qm5 forms the Upper Maqrah basalt. The characteristics of the stratigraphic units are summarized below in stratigraphic order.

Quaternary upper Maqrah basalt (lacking erosion)

Qm5, historic to late prehistoric lava flows and scoria cones

The subunit comprises the products of four eruption sites of black scoria cones with lava flows with surrounding

mantles of black air fall ash still covering adjacent steep hillsides often of Precambrian basement standing through the lava field. One of these sites is believed to have erupted in the 10th Century; about 1000 years ago (Catalogue of the Active Volcanoes of the World, Part XVI Arabia and the Indian Ocean - International Association of Volcanology, 1963). The present field study suggested that this is most likely Harrat Maqrah but care needs to be exercised as all older cones nearby are mantled in air fall ash and look like the youngest cone which can be distinguished by a ring of large rounded cannon-ball basaltic bombs around its base.

Qm4, prehistoric lava flows and scoria cones

Lacks erosion and has dust ponds of 3 m in diameter. Very black color on aerial photographs and satellite images.

Quaternary lower Maqrah basalt (with erosion)

Qm3: Non-eroded lava flows, slight gulling on scoria cones, dust ponds up to 100 m in diameter.

Qm2: Eroded lava flows and scoria cones, surface structures on flows such as flow ridges intact, but erosional rivulets are present. Scoria cones have distinct gullies and dust ponds are up to 400m in diameter.

Qm1, Eroded lava flows, surface structures on flows are removed by erosion, but edges of flows are distinct. Scoria cones are deeply eroded but the craters remain distinct.

Unconformity (with laterite surface)

Tertiary Jarad basalt

Tj, deeply eroded and smoothed lava flows, individual flows no longer distinct. Scoria cones are deeply eroded to red scoria interiors with craters indistinct or removed by erosion.

Sediments

Qal, Wadi gravels

Qe, Aeolian sands

Qsb, Sabkah/ dust pond

QTu, quaternary to tertiary terrace deposits of rounded boulders, gravels and sand.

Precambrian shield

Pc, upper proterozoic metavolcanic rocks and plutons mainly granitic. These rise as rugged hills around and within the lavas of Harrat Lunayyir. Scoria cones are

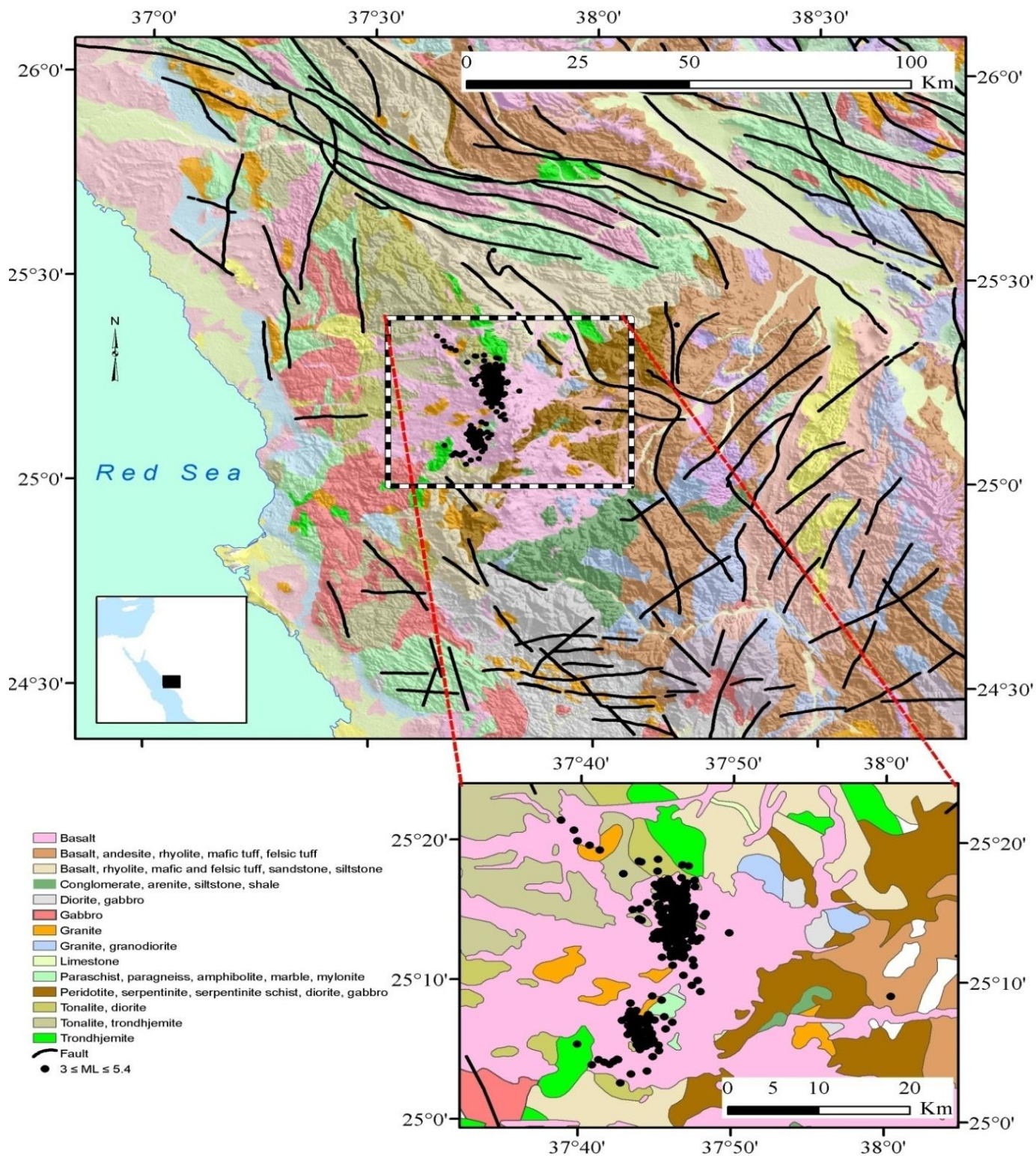


Figure 3. Geotectonic map shows different geologic units along with structural lineaments and epicentral locations (Al-Amri and Fnais, 2009).

commonly found on the tops of granite hills with lava flows draping the sides of the hills. The light colored

granite hills clearly show their remnant mantles of black basaltic air fall ashes from the historic to late prehistoric

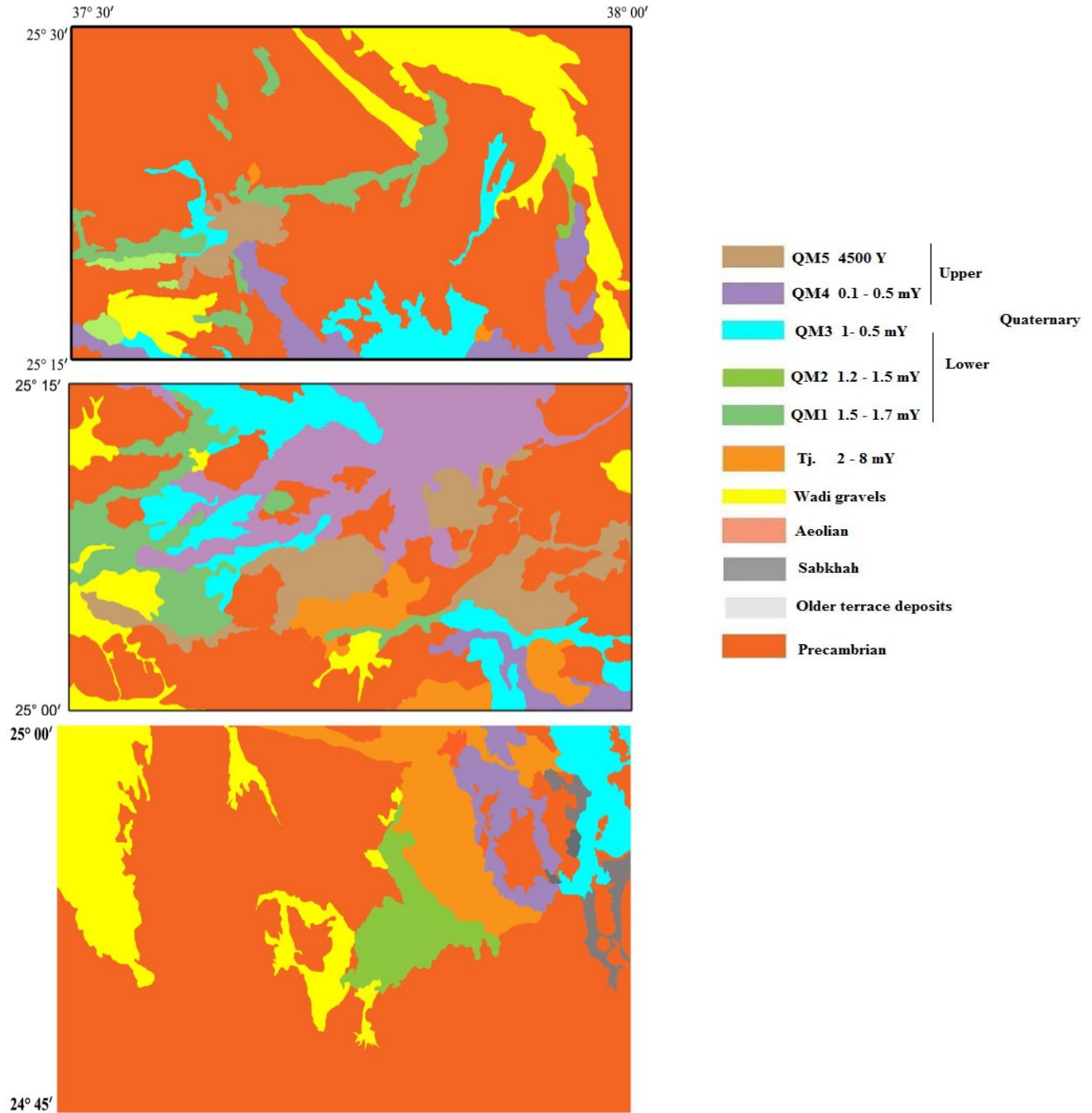


Figure 4. Geological maps of Harrat Lunayyir show areal distribution of volcanic flows.

eruptions.

METHODOLOGY

⁴⁰Ar - ³⁹Ar age determinations

Prior to this study no age determinations had been produced for Harrat Lunayyir lavas. During the mapping the volcanic stratigraphy was proposed, using the same erosional characteristics as were used in an earlier study of Harrat Rahat (Camp et al., 1989a). The

stratigraphic units are believed to be of broadly similar ages (Roobol, personal communication, 2011). An estimate made in this manner for the stratigraphic units of Harrat Lunayyir prior to laboratory dating is given as follows.

Quaternary Maqrah basalt

- Qm5, Historic to late prehistoric. Less than 4,500 years.
- Qm4: 0.1 to 0.5 Ma
- Qm3: 0.5 to 1.0 Ma

Qm2: 1.2 to 1.5 Ma
Qm1: 1.5 to 1.7 Ma

Tertiary Jarad basalt

Tj: 2.0 to 8.0 Ma

$^{40}\text{Ar}/^{39}\text{Ar}$ age determinations were carried out at the TerraChron Corporation Geochronology Laboratory, Toronto, Canada. Each sample was labeled with a HL sample number. The general appearance and physical characteristics of the samples have been examined, and portions were then selected for argon isotopic analysis. These selected portions were crushed, sieved and then examined under the binocular microscope to identify the basic phases and to select grains for irradiation.

The selected rock chips were packaged in aluminum foil and loaded into an aluminum canister, together with a number of grains of the sanidine standard FCT and the Beloc tektite standard, and irradiated in the McMaster Nuclear Reactor, Hamilton, Ontario. The samples were irradiated for a total of 48 Megawatt-hours (~16 h in the reactor). After cooling of short-lived radionuclides the samples and standards were placed into holes in an aluminum disk and loaded into the ultra-high vacuum sample chamber within the mass spectrometer inlet system. After pumping down, the sample chamber and gas extraction line were baked for at least 12 h at 150°C to achieve low argon blank levels. The analyses reported here were performed in a single loading of the mass spectrometer. The first stage in the analysis was to fuse each of the standards in a single heating step, using a Lee Laser Nd-YAG laser operated with frequency doubling, to produce green light of 532 nm wavelength. The diffused gas was then purified by an SAES type 707 Ti-Fe-Zr getter held at 250°C to remove all reactive gases. The remaining noble gas component was let into a VG1200 mass spectrometer equipped with an ion multiplier for isotopic analysis of argon. The mass spectrometer was operated in static mode, isolated from the pumps during the analysis. All five natural and irradiation-produced argon isotopes (^{36}Ar through ^{40}Ar) were measured in 20 to 40 successive cycles over about a one-hour period, followed by pumping out of the mass spectrometer. Procedural blanks (in which all steps except the laser heating were followed) were performed before each analysis. The resulting argon isotope measurements were reduced using software developed in-house, which includes correction for atmospheric contamination, mass discrimination and for interfering nuclear reactions resulting from the irradiation, as well as appropriate statistical analysis of the data, including a detailed treatment of error propagation. The J value (efficiency of ^{39}Ar production from ^{39}K) was calculated for each standard, using an age of 66.0 Ma for the tektite standard. The J value varies with its position in the container during irradiation and standards are distributed along the length of the container. Each sample analyzed was assigned an appropriate J value for the irradiation, depending on its own position in the irradiation container. The samples were analyzed in an identical procedure, except for Ar which was extracted in a series of heating steps. In each heating step, the sample was heated by the laser, generally for 30 s, followed by the gas purification and analysis steps as above. In successive heating steps the laser power was gradually increased until the sample was fused in the final step.

RESULTS AND DISCUSSION

Integrated (Total-gas) age

The age obtained by mathematically summing all of the argon gas fractions extracted during a step-heating

analysis. It is essentially equivalent to a traditional K-Ar age, though with somewhat higher precision because it does not require the independent analysis for K-content necessary in K-Ar analysis. It is also essentially equivalent to a single-step analysis in $^{40}\text{Ar}/^{39}\text{Ar}$ dating, where all of the sample argon is extracted in a single heating step.

Plateau age

The age obtained by combining several successive heating steps in a step-heating argon analysis. The successive steps to be combined should ideally have ages that are indistinguishable within the analytical errors of the individual steps, and should represent a significant fraction of the total sample argon. On a diagram of age vs. cumulative proportion of ^{39}Ar released, these successive concordant ages appear as a horizontal plateau, hence the name. Ages in this type of diagram are normally computed assuming all sample ^{36}Ar measured is derived from atmosphere. A measure of how well the measured points fit the plateau is given by the goodness-of-fit parameter referred to here as $S/(n-1)$. For a well-fitted plateau this number should be close to one, while significantly larger values indicate a poorer fit.

Isochron age

The age obtained by fitting a straight line through several successive heating step compositions, as plotted on a diagram of $^{36}\text{Ar}/^{40}\text{Ar}$ vs. $^{39}\text{Ar}/^{40}\text{Ar}$. The successive steps to be combined should fit the line within the analytical errors of the individual steps, and should represent a significant fraction of the total sample argon. The intercept of the line with the $^{39}\text{Ar}/^{40}\text{Ar}$ axis corresponds to an age, while its intercept with the $^{36}\text{Ar}/^{40}\text{Ar}$ axis gives the initial $^{36}\text{Ar}/^{40}\text{Ar}$ ratio at that time. The isochron treatment is useful when the conventional age spectrum (which is based on the assumption that the initial $^{36}\text{Ar}/^{40}\text{Ar}$ ratio was that of modern atmosphere) fails to define a plateau age. In this case, if an isochron nevertheless exists with a non-atmospheric $^{36}\text{Ar}/^{40}\text{Ar}$ ratio, it may indicate a reliable crystallization age. In that case, the initial argon ratio gives the ambient argon composition at that time – usually greater than the atmospheric value ($^{40}\text{Ar}/^{36}\text{Ar} = 295.5$), and attributed to mantle-derived Ar carried in phenocryst phases such as olivine and clinopyroxene. As with the plateau, a measure of how well the measured points fit the isochron line is given by the goodness-of-fit parameter referred to here as $S/(n-1)$. For a well-fitted isochron, this number should be close to one; while significantly larger values indicate a poor fit.

HL-2

A whole rock chip (P53-035) run in 11 steps gives an

integrated age of -50 ± 118 ka, with integrated Ca/K ratio of 5.59 ± 0.01 . This integrated age is essentially zero, as the measured integrated $^{40}\text{Ar}/^{36}\text{Ar}$ of 295.2 ± 0.6 is not significantly different from that of the atmospheric value (Figure 5). Step-heating can potentially improve the radiogenic argon yield (that is give higher values of $^{40}\text{Ar}/^{36}\text{Ar}$) because the atmospheric argon is often more loosely bound to the mineral surfaces and can be preferentially extracted in low temperature steps. This heating can result in more radiogenic fractions derived from middle to higher temperature steps. Indeed the $^{36}\text{Ar}/^{40}\text{Ar}$ vs. $^{39}\text{Ar}/^{40}\text{Ar}$ correlation plot shows that the step-heating successfully produced fractions with progressively higher potassium to argon ratios, as shown by higher $^{39}\text{Ar}/^{40}\text{Ar}$ values (the highest temperature step 11 has the highest $^{39}\text{Ar}/^{40}\text{Ar}$ ratio). Nonetheless, in this case none of the 11 steps have $^{40}\text{Ar}/^{36}\text{Ar}$ ratios that are significantly higher than 295.5. Thus on this plot, all points fit a line within uncertainties [$S/(n-1) = 0.58$], and give a Y-intercept corresponding to a $^{40}\text{Ar}/^{36}\text{Ar}$ ratio of 295.0 ± 0.8 , in agreement with the atmospheric ratio. But the line has essentially zero slopes, and poorly constrained $^{39}\text{Ar}/^{40}\text{Ar}$ intercept that corresponds to an isochron age of 5 ± 81 ka, signifying the very recent crystallization of this rock.

HL-14

A whole rock chip (P53-022) run in 10 steps gives an integrated age of 478 ± 113 ka, with integrated Ca/K ratio of 5.83 ± 0.01 . In contrast to HL-2 (above) the integrated $^{40}\text{Ar}/^{36}\text{Ar}$ ratio of 301.7 ± 1.5 is slightly but significantly above the atmospheric ratio of 295.5 and consequently a positive age has been measured (Figure 5). Although the step radiogenic yields are significantly higher than those in sample HL-2, they are still low (less than 5% radiogenic ^{40}Ar). An age spectrum for the sample is made by assuming that the non-radiogenic Ar in each step has $^{40}\text{Ar}/^{36}\text{Ar}$ ratios of 295.5. At these low proportions of radiogenic ^{40}Ar the calculated ages are very sensitive to small departures from the assumed $^{40}\text{Ar}/^{36}\text{Ar}$ ratio of 295.5. Thus caution must be used in the interpretation of both the integrated age and the step ages. The uncertainties in each age are relatively large (again reflecting the small amounts of radiogenic argon). However, within the uncertainties the age spectrum is uniformly flat. This stands in contrast to the Ca/K spectrum that begins at a ratio of 2.01 and climbs to a final value of 9.95 ± 0.06 .

In contrast to the integrated age and the plateau age calculated from the step compositions, a free fit of the data on the $^{36}\text{Ar}/^{40}\text{Ar}$ vs. $^{39}\text{Ar}/^{40}\text{Ar}$ correlation plot makes no assumption about the isotopic composition of the non-radiogenic argon and thus may be a preferable means of age calculation for non-radiogenic samples. On this plot all of the points fit a line within experimental uncertainties [$S/(n-2) = 0.52$] corresponding to an isochron age of

534 ± 343 ka, with a calculated initial $^{40}\text{Ar}/^{36}\text{Ar}$ ratio of 295.2 ± 4.3 . This calculated initial ratio is indistinguishable from the modern atmospheric ratio of 295.5. Accordingly, a degree of freedom could be used to fix the initial ratio on this plot at 295.5 (actually $1/295.5$, this corresponds to "NIER" on the plot) and refit the points. Treated this way, the points still fit the line within uncertainties [$S/(n-1) = 0.46$] and constrain the age to 511 ± 78 ka. As the levels of radiogenic argon are similarly low in the remaining four analyses, we regard the results derived from the isotope correlation plot to be most appropriate means to estimate the ages of these samples.

HL-17

A whole rock chip (P53-034) run in 16 steps gives an integrated age of 172 ± 304 ka, with integrated Ca/K ratio of 7.39 ± 0.02 . Its Ca/K spectrum climbs gradually from 3.1 ± 0.2 (step 1) to a mid-temperature plateau averaging 6.66 ± 0.16 (steps 7 to 13) before climbing steeply to a final value of 22.0 ± 0.1 (step 16). On the $^{36}\text{Ar}/^{40}\text{Ar}$ vs. $^{39}\text{Ar}/^{40}\text{Ar}$ plot (Figure 6), a free fit of all of the points yields an isochron age of 518 ± 223 ka [$S/(n-1) = 0.32$], with an atmospheric initial $^{40}\text{Ar}/^{36}\text{Ar}$ ratio of 294.6 ± 1.0 . The same data forced through the atmospheric $^{40}\text{Ar}/^{36}\text{Ar}$ ratio of 295.5 yield an isochron [$S/(n-1) = 0.36$] corresponding to an age of 325 ± 89 ka.

HL-26

A whole rock chip (P53-033) run in 8 steps gives an integrated age of 352 ± 111 ka, with integrated Ca/K ratio of 9.75 ± 0.02 . Its age spectrum is uniform except for the final fraction 8 that yields a significantly older apparent age of 2.6 ± 0.9 Ma (Figure 6). This old age is also correlated with a significantly high Ca/K value of 34.0 ± 0.3 . Steps 1 through 6 on the Ca/K spectrum have relatively uniform values averaging 5.8 ± 0.3 . On the $^{36}\text{Ar}/^{40}\text{Ar}$ vs. $^{39}\text{Ar}/^{40}\text{Ar}$ plot, a free fit of steps 1 to 7 yields an isochron age of 116 ± 143 ka [$S/(n-1) = 0.10$], with an atmospheric initial $^{40}\text{Ar}/^{36}\text{Ar}$ ratio of 296.6 ± 1.7 . The same data forced through the atmospheric $^{40}\text{Ar}/^{36}\text{Ar}$ ratio of 295.5 yield an isochron [$S/(n-1) = 1.046$] corresponding to an age of 209 ± 85 ka. The age from step 8 (green) lies significantly below this isochron.

HL-31

A whole rock chip (P53-029) run in 11 steps gives an integrated age of 277 ± 121 ka, with integrated Ca/K ratio of 5.16 ± 0.01 . On the Ca/K plot, Ca/K ratios increase from 1.96 ± 0.14 (step 1) to 8.05 ± 0.02 in the final step. On the $^{36}\text{Ar}/^{40}\text{Ar}$ vs. $^{39}\text{Ar}/^{40}\text{Ar}$ plot (Figure 7), the step compositions fit an isochron within the experimental

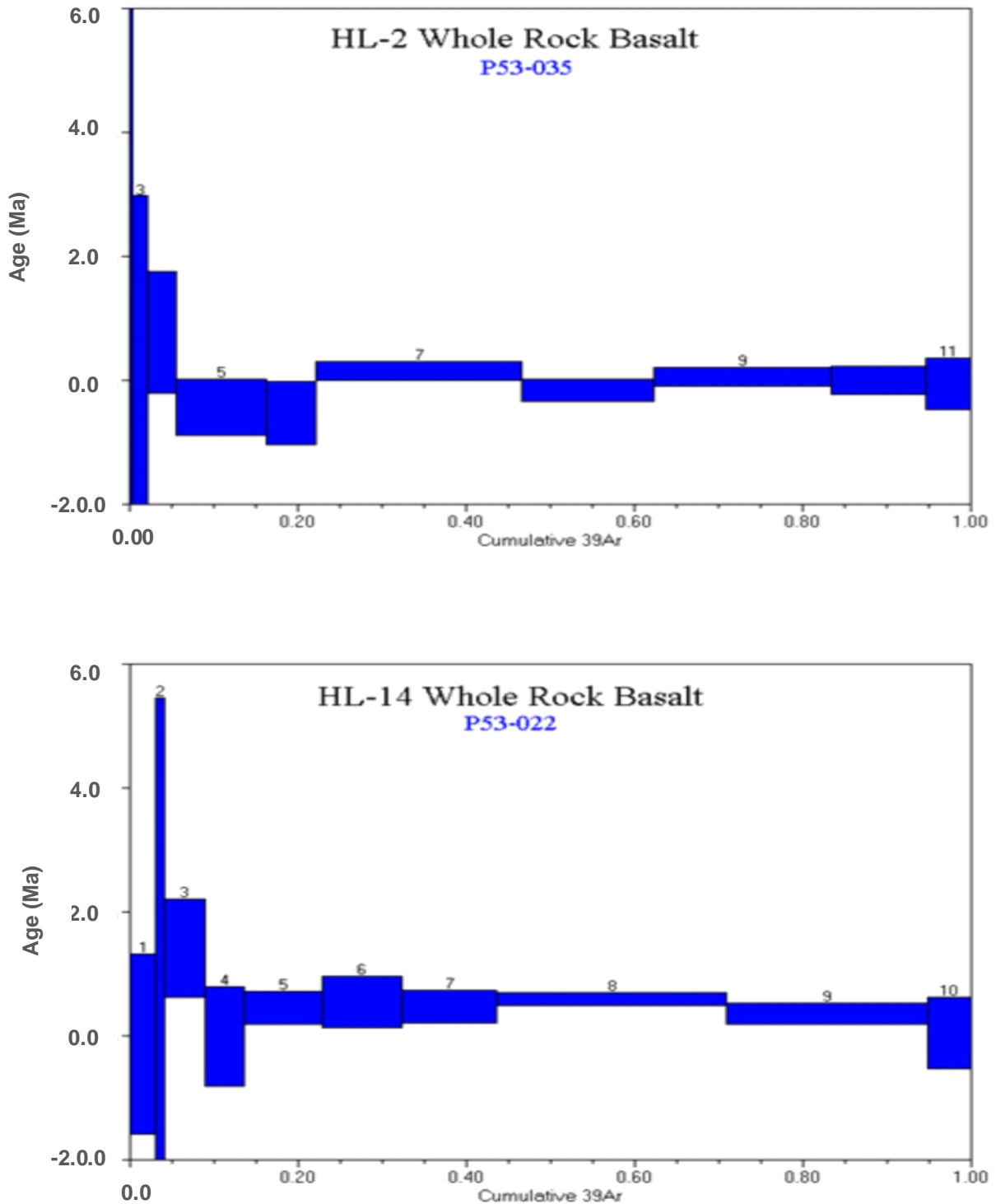


Figure 5. $^{40}\text{Ar}/^{39}\text{Ar}$ incremental heating release spectra for samples HL-2 and HL-14.

uncertainties [$S/(n-1) = 0.48$] corresponding to an age of 126 ± 557 ka, with an atmospheric initial $^{40}\text{Ar}/^{36}\text{Ar}$ ratio of 297.0 ± 6.5 . The same data forced through the atmospheric $^{40}\text{Ar}/^{36}\text{Ar}$ ratio of 295.5 yield an isochron [$S/(n-1) = 0.44$] corresponding to an age of 256 ± 83 ka.

HL-35

A whole rock chip (P53-027) run in 11 steps gives an integrated age of 95 ± 109 ka, with integrated Ca/K ratio of 4.75 ± 0.01 . Its Ca/K spectrum starts at a ratio of $2.54 \pm$

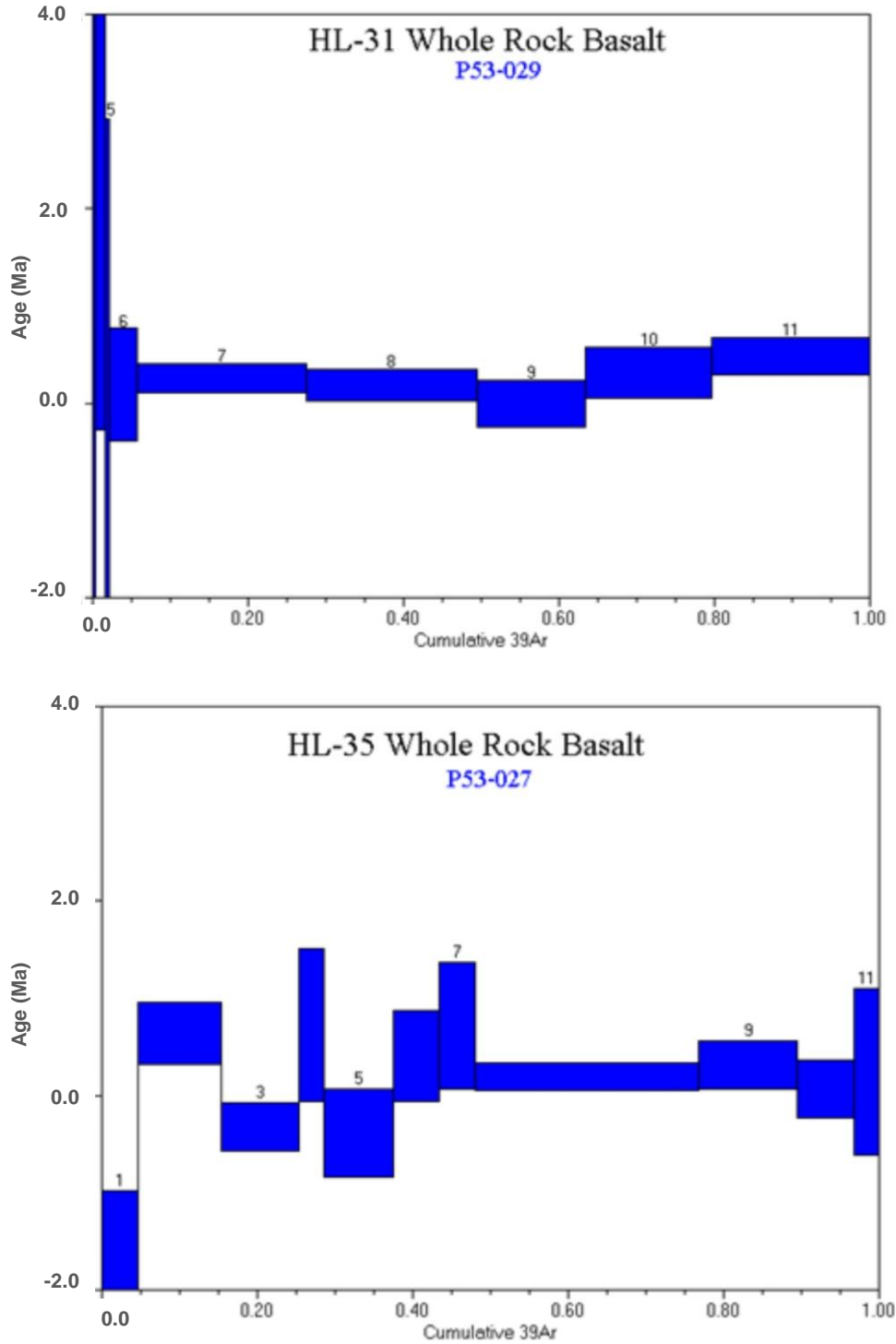


Figure 6. $^{40}\text{Ar}/^{39}\text{Ar}$ incremental heating release spectra for samples HL-17 and HL-26.

0.03 climbs to a plateau averaging 4.33 ± 0.06 , before rising to 12.78 ± 0.07 in the final fraction. On the $^{36}\text{Ar}/^{40}\text{Ar}$ vs. $^{39}\text{Ar}/^{40}\text{Ar}$ plot (Figure 7), a free fit of all of the points yields an isochron age of 368 ± 203 ka [$S/(n-1) = 1.41$], with an atmospheric initial $^{40}\text{Ar}/^{36}\text{Ar}$ ratio of 294.0 ± 1.5 . The same data forced through the atmospheric $^{40}\text{Ar}/^{36}\text{Ar}$

ratio of 295.5 give an isochron age of 325 ± 89 ka (Table 1). The $S/(n-1)$ value of 1.42 indicates the points scatter very slightly outside of analytical uncertainties. The uncertainty on the corresponding isochron age of 149 ± 130 ka has been adjusted for the slight scatter of the data points.

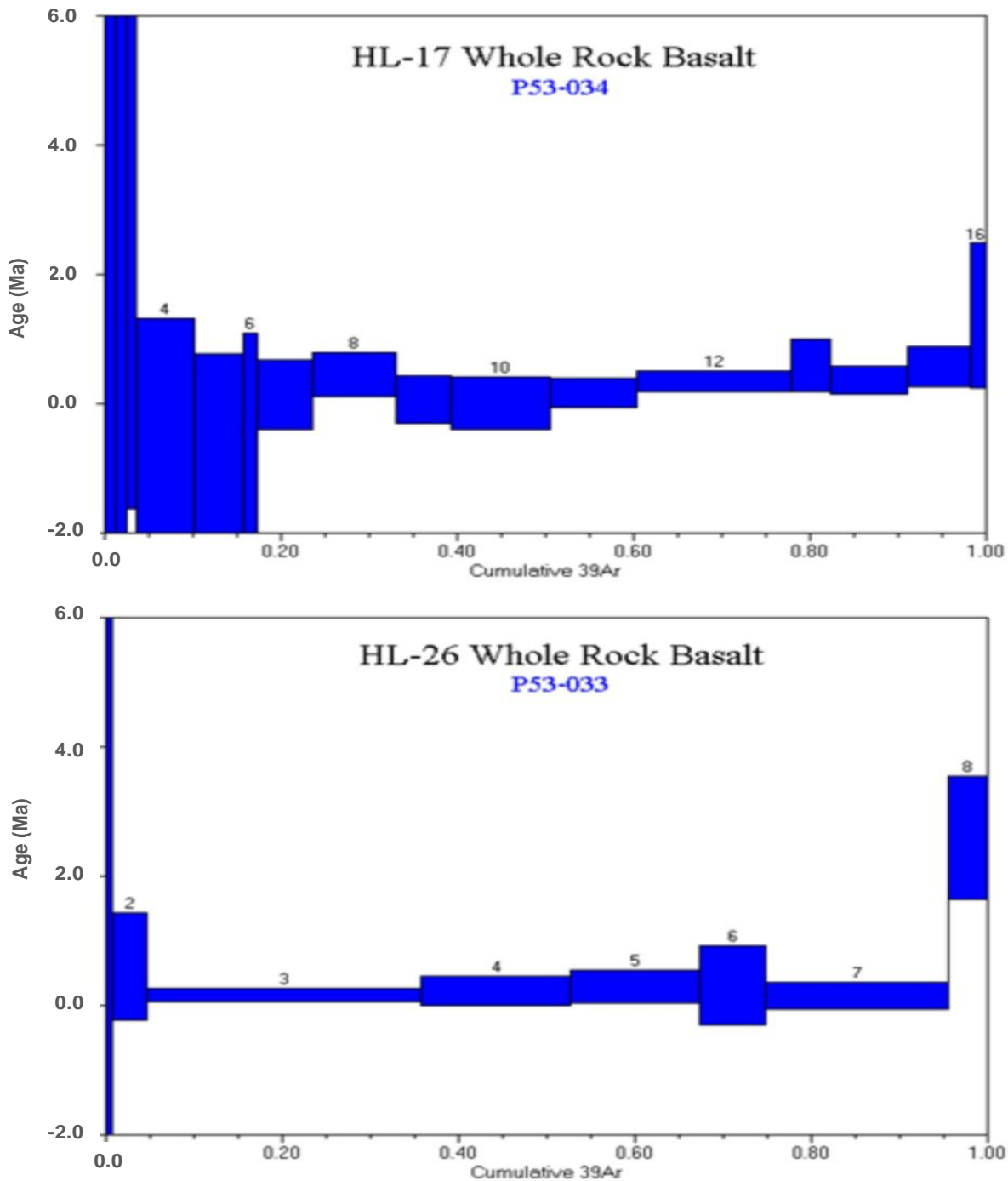


Figure 7. $^{40}\text{Ar}/^{39}\text{Ar}$ incremental heating release spectra for samples HL-31 and HL-35.

Generally, it is apparent from the plots of Ca/K that in all six samples Ca-rich phases predominate at the highest temperatures. This is a common feature in basaltic rocks. Only in sample HL-26 is there an indication that a high Ca/K phase may be correlated with a relict or older age. The other samples yield uniform apparent ages throughout their respective age-spectra in spite of the widely varying Ca/K ratios. Thus, the ages can be

considered to be representative.

Prior to these analyses, estimates of the ages of the samples were cited as Tertiary to Quaternary. This work places the ages of all six samples firmly in the Quaternary period. Their ages have been summarized in the Figure 8. The precision of the ages calculated in this study is limited by the small amounts of radiogenic argon compared to the larger amounts of non-radiogenic or

Table 1. Summary of analytical results from ⁴⁰Ar/³⁹Ar incremental heating experiments.

Sample number	U of T analysis	Type of material	Number of steps	Integrated age (ka)	Wt. mean (preferred) age (ka)	Ca/K ratio	Method	⁴⁰ Ar/ ³⁶ Ar	$\sum \chi^2 / f$ ($\nu - \phi$)
HL-2 (Q5)	P53-035	Whole rock	11	-50 ± 118	5 ± 81	5.59 ± 0.01	Isochron	295.5	0.58
HL-14 (Q2)	P53-022	Whole rock	10	478 ± 113	511 ± 78	5.83 ± 0.01	Isochron	295.5	0.46
HL-17 (T)	P53-034	Whole rock	16	172 ± 304	325 ± 89	7.39 ± 0.02	Isochron	295.5	0.36
HL-26 (Q4)	P53-033	Whole rock	8	352 ± 111	209 ± 85	9.75 ± 0.02	Isochron	295.5	1.046
HL-31 (Q1)	P53-029	Whole rock	11	277 ± 121	256 ± 83	5.16 ± 0.01	Isochron	295.5	0.44
HL-35 (Q3)	P53-027	Whole rock	11	95 ± 109	149 ± 130	4.75 ± 0.01	Isochron	295.5	1.42

*, Goodness-of-fit parameter; f, degrees of freedom: f = 1 for isochrons forced through 295.5.

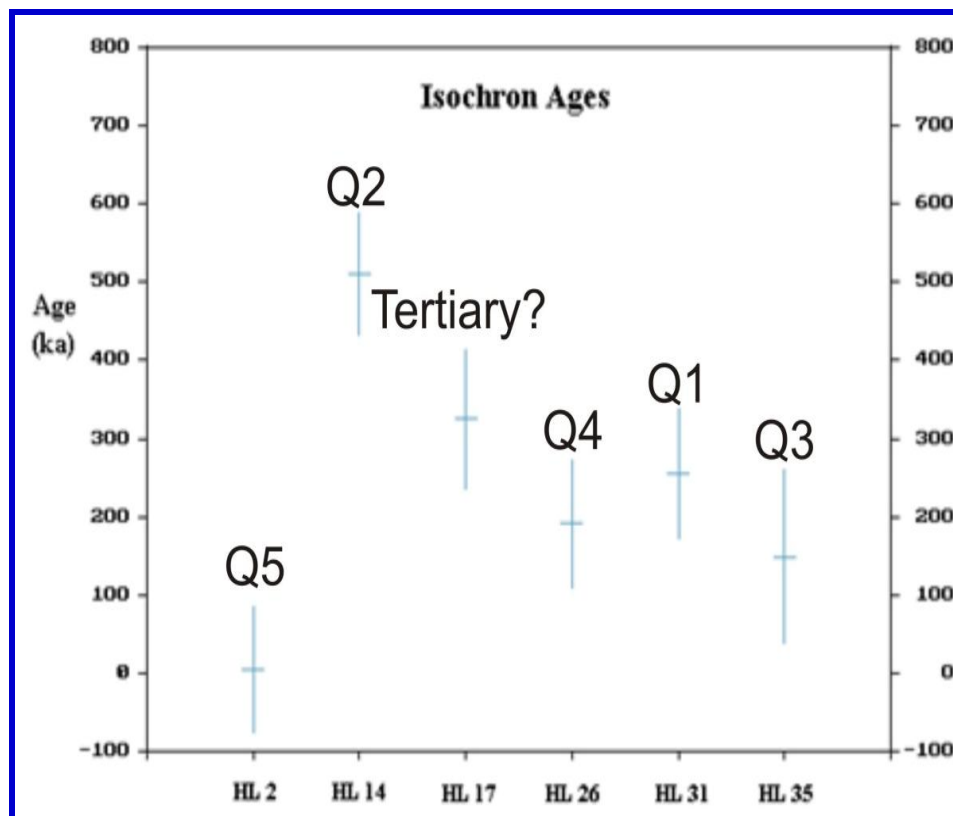


Figure 8. Isochron ages for all samples.

atmospheric argon typical in basaltic whole rocks of this age.

Conclusions

Geologically, Harrat Lunayyir is a very young volcanic region composed of late Neogene and Quaternary basaltic lavas and pyroclastics directly overlying deeply eroded Neoproterozoic rocks of the Arabian Shield. It is one of the smallest of the Holocene lava fields of Saudi Arabia, but individual flow lobes radiate long distances from the center of the Harrat, and flows reached the Red Sea in two places. One of the cones may have erupted around the 10th century AD or earlier. The lava field lies about 200 km east of the spreading center under the Red Sea. Harrat Lunayyir possibly owes its existence to mantle melting along the margin of this upwelling system.

The dominantly basaltic lavas of Harrat Lunayyir have been divided on and the basis of erosional characteristics into two major units – an older Tertiary unit (Jarad basalt), and a younger Quaternary unit (Maqrah basalt). The Quaternary Maqrah basalt has been subdivided into five stratigraphic subunits, Qm1 and Qm2 forming the Lower Maqrah basalt and Qm3, Qm4, and Qm5 forming the Upper Maqrah basalt.

During episodes of volcanic activity the relief of the Precambrian basement was great enough to hinder the basalt flow westwards. Detailed investigation of the basalts leads to the identification of the following succession:

- Historic to Late Prehistoric lava flows.
- Prehistoric lava flows and scoria cones.
- Non eroded lava flows and scoria cones.
- Eroded lava flows and scoria cones.
- Eroded lava flows
- Unconformity.
- Tertiary basalt.

Generally speaking, it is apparent from the plots of Ca/K that in all six samples Ca-rich phases predominate at the highest temperatures. This is a common feature in basaltic rocks. Only in sample HL-26 is there is an indication that a high Ca/K phase may be correlated with a relict or older age. The other samples yield uniform apparent ages throughout their respective age-spectra in spite of the widely varying Ca/K ratios. Thus, the ages can be considered to be reliable.

Prior to these analyses, estimates of the ages of the samples were cited as Tertiary to Quaternary. This work places the ages of all six samples firmly in the Quaternary period. The precision of the ages calculated in this study are limited by the small amounts of radiogenic argon compared to the larger amounts of non-radiogenic or atmospheric argon typical in basaltic whole rocks of this age. The discrepancies in ages and

stratigraphic position are due to the small amounts in accumulated argon over the relatively very short period of time. The volcanic activity at Harrat Lunayyir started about 500 000 years ago. There must have been a substantial time between the lowest unit (which has previously assigned a Tertiary age) and Q1 so that an unconformity has been developed. The last activity could have taken place at about 5000 years ago.

ACKNOWLEDGMENTS

The authors would like to express their thanks and gratitude to King Abdulaziz City for Science and Technology for funding the project AR-28 – 95 and to Drs. John Roobol and Ghaleb Jarrar for their Drs. John Roobol and Ghaleb Jarrar for their consultation and guidance.

REFERENCES

- Al-Amri AM, Fnais MS (2009) Seismo-volcanic investigation of 2009 earthquake swarms at Harrat Lunayyir (Ash Shaqah), Western Saudi Arabia. *Int. J. Earth Sci. Eng., India* (in press).
- Al-Damegh K, Sandvol E, Barazangi M (2005). Crustal structure of the Arabian plate: New constraints from the analysis of teleseismic receiver functions. *Earth Planet. Sci. Lett.*, (231): 177-196.
- Baer G, Hamiel Y (2010). Form and growth of an embryonic continental rift: InSAR observations and modelling of the 2009 western Arabia rifting episode. *Geophys. J. Int.*, 182: 155-167 doi: 10.1111/j.1365-246X.2010.04627.
- Barazangi M (1981). Evaluation of seismic risk along the western part of the Arabian plate: discussion and recommendations, *Bull. Fac. Earth Sci., King Abdulaziz Univ., Jiddah, K.S.A.*, 4: 77-87.
- Benoit MH, Nyblade AA, VanDecar JC, Gurrrola H (2003). Upper mantle P wave velocity structure and transition zone thickness beneath the Arabian Shield. *Geophys. Res. Lett.*, 30: 1-4.
- Camp VE, Roobol MJ (1992). Upwelling asthenosphere beneath western Arabia and its regional implications: *J. Geophys. Res.*, 97(15): 255-271.
- Camp VE, Hooper PR, Roobol MJ, White DL (1987). The Madinah eruption, Saudi Arabia: Magma mixing and simultaneous extrusion of three basaltic chemical types: *Bull. Volcanol.*, 49: 489-508.
- Camp VE, Roobol VE, Hooper PR (1989a). The Arabian continental alkali basalt province: Part I. Evolution of Harrat Rahat, Kingdom of Saudi Arabia: *Bull. Geol. Soc. Am.*, 101: 71-95.
- Camp VE, Roobol MJ, Hooper PR (1989). Intraplate alkalic volcanism and magmatic processes along the v600km-long Makkah-Madinah-Nafud volcanic line, western Saudi Arabia: General Assembly of the International association of Volcanology and Chemistry of the Earth's Interior, Continental Magmatism Abstracts, New Mexico Bureau of Mines and Min. Res. Bull., 131: 49.
- Daradich A, Mitrovica JX, Pysklywec RN, Willett SD, Forte AM (2003). Mantle flow, dynamic topography, and rift-flank uplift to Arabian. *Geol. Soc. Am.*, 31: 901-904.
- Girdler RW (1969). The Red Sea-a geophysical background. In: Degens ET, Ross D. A. (eds): Hot brines and recent heavy metal deposits in the Red Sea. Springer, New York, pp. 59-70
- Johnson PR (1998). Tectonic map of Saudi Arabia and adjacent areas. Deputy Ministry for Mineral Resources Technical Report USGS-TR-98-3 (IR 948).
- Jónsson S, Pallister J, McCausl W, El-Hadidy S (2010). Dyke Intrusion and Arrest in Harrat Lunayyir, western Saudi Arabia, in April-July 2009. *Geophysical Research Abstracts*, 12: 32. EGU2010-7704.
- Julia J, Ammon C, Herrmann R (2003). Lithosphere structure of the

- Arabian Shield from the joint inversion of receiver functions and surface-wave group velocities. *Tectonophysics*, 371: 1-21
- Kinkar A, Shawali AA, Bankher KA, End E, Roobol MJ, Wynn J (1994b). The Al-Madinah-Harrat Rahat volcanic monitoring project summary report. Saudi Arabian Deputy Ministry for Mineral Resources Confidential Report USGS-CR-94-1 (IR909), p. 47.
- Moufti MRH, Hashad MH (2005). Volcanic hazards assessment of Saudi Arabian Harrats: geochemical and isotopic studies of selected areas of active Makkah- Madinah-Nafud (MMN) volcanic rocks. Final Project Report (LGP-5-27), King Abdulaziz City for Science and Technology, Riyadh, Saudi Arabia.
- Pallister J, McCausland W, Jónsson S, Lu Z, Zahran HM, El-Hadidy S, Aburukbah A, Stewart I, Lundgern P, White R, Moufti M (2010). Broad accommodation of rift-related extension recorded by dike intrusion in Saudi Arabia. *Nature Geosciences*, Macmillan Publishers Limited, p. 8.
- Poirier JP, Taher MA (1980). Historical seismicity in the near and middle east, north Africa, and Spain from Arabic documents (VIIth-XVIII century), *Bull. Seis. Soc. Am.*, 70(6): 2185-2201.
- Roobol MJ, Al-Rehaili M (1997). Geohazards along the Makkah-Madinah-Nafud (MMN) volcanic line: Saudi Arabian Deputy Ministry for Mineral Resources Technical Report DMMR-TR-97-1: 125-140.
- Roobol MJ, Bankher K, Bamufleh S (1994). Geothermal anomalies along the MMN volcanic line including the cities of Al-Madinah Al-Munawwarah and Makkah Al-Mukarramah. Saudi Arabian Deputy Ministry for Mineral Resources Confidential Report DGMR-MADINAH- CR-15-2, p. 95.
- SGS (2005). Technical work program of the Saudi Geological Survey (SGS), Jeddah, Saudi Arabia. p. 79.
- Stoeser DB, Camp VE (1985). Pan-African microplate accretion of the Arabian Shield, *Bull. Geol. Soc. Am.*, 6: 817-826.
- Trilling RI, Heliker C, Swanson DA (2010). Eruptions of Hawaiian Volcanoes, past, present and future: U.S. Geological Survey General information product, 117: 63.
- Zobin VM (2003). Introduction to volcanic seismology. Elsevier Publications. www.elsevierdirect.com.
- Zobin VM, Al-Amri AM, Fnais M (2011). Seismicity associated with active, new-born, and re-awakening basaltic volcanoes: case review and the possible scenarios for the Harraat volcanic provinces, Saudi Arabia. *Arabian J. Geosci.*, Vol. 4. DOI: 10.1007/s12517-011-0379-3.